


## RESEARCH ARTICLE

# Multishell diffusion MRI reveals whole-brain white matter changes in HIV

Silvia Minosse<sup>1</sup> | Eliseo Picchi<sup>1,2</sup> | Allegra Conti<sup>2</sup> | Francesca di Giuliano<sup>2,3</sup> |  
Francesco di Cìò<sup>2</sup> | Loredana Sarmati<sup>4,5</sup> | Elisabetta Teti<sup>4</sup> | Silvia de Santis<sup>6</sup> |  
Massimo Andreoni<sup>4,5</sup> | Roberto Floris<sup>1,2</sup> | Maria Guerrisi<sup>2</sup> |  
Francesco Garaci<sup>2,3,7</sup> | Nicola Toschi<sup>3,8</sup> 

<sup>1</sup>Diagnostic Imaging Unit, University Hospital Rome Tor Vergata, Rome, Italy

<sup>2</sup>Department of Biomedicine and Prevention, University of Rome Tor Vergata, Rome, Italy

<sup>3</sup>Neuroradiology Unit, University Hospital of Rome Tor Vergata, Rome, Italy

<sup>4</sup>Clinical Infectious Diseases Unit, University Hospital of Rome Tor Vergata, Rome, Italy

<sup>5</sup>Department of Systems Medicine, University of Rome Tor Vergata, Rome, Italy

<sup>6</sup>Instituto de Neurociencias, Consejo Superior de Investigaciones Científicas and Universidad Miguel Hernández, Sant Joan d'Alacant, Spain

<sup>7</sup>IRCSS San Raffaele Cassino, Frosinone, Italy

<sup>8</sup>Athinoula A. Martinos Center for Biomedical Imaging, Harvard Medical School, Boston, Massachusetts, USA

## Correspondence

Nicola Toschi, Medical Physics Section, Department of Biomedicine and Prevention, Via Montpellier 1, 00133 Rome, Italy.  
Email: [toschi@med.uniroma2.it](mailto:toschi@med.uniroma2.it)

## Funding information

Project BRAINSTORM, Grant/Award Number: 101099355; Project EXPERIENCE, Grant/Award Number: 101017727

## Abstract

Diffusion tensor imaging (DTI) and diffusion kurtosis imaging (DKI) have been previously used to explore white matter related to human immunodeficiency virus (HIV) infection. While DTI and DKI suffer from low specificity, the Combined Hindered and Restricted Model of Diffusion (CHARMED) provides additional microstructural specificity. We used these three models to evaluate microstructural differences between 35 HIV-positive patients without neurological impairment and 20 healthy controls who underwent diffusion-weighted imaging using three *b*-values. While significant group effects were found in all diffusion metrics, CHARMED and DKI analyses uncovered wider involvement (80% vs. 20%) of all white matter tracts in HIV infection compared with DTI. In restricted fraction (FR) analysis, we found significant differences in the left corticospinal tract, middle cerebellar peduncle, right inferior cerebellar peduncle, right corticospinal tract, splenium of the corpus callosum, left superior cerebellar peduncle, left superior cerebellar peduncle, pontine crossing tract, left posterior limb of the internal capsule, and left/right medial lemniscus. These are involved in language, motor, equilibrium, behavior, and proprioception, supporting the functional integration that is frequently impaired in HIV-positivity. Additionally, we employed a machine learning algorithm (XGBoost) to discriminate HIV-positive patients from healthy controls using DTI and CHARMED metrics on an ROIwise basis, and unique contributions to this discrimination were examined using Shapley Explanation values. The CHARMED and DKI estimates produced the best performance. Our results suggest that biophysical multishell imaging, combining additional sensitivity and built-in specificity, provides further information about the brain microstructural changes in multimodal areas involved in attentive, emotional and memory networks often impaired in HIV patients.

Silvia Minosse and Eliseo Picchi have contributed equally to this study.

This is an open access article under the terms of the [Creative Commons Attribution-NonCommercial-NoDerivs](https://creativecommons.org/licenses/by-nc-nd/4.0/) License, which permits use and distribution in any medium, provided the original work is properly cited, the use is non-commercial and no modifications or adaptations are made.

© 2023 The Authors. *Human Brain Mapping* published by Wiley Periodicals LLC.

## KEYWORDS

explainability, machine learning, multishell diffusion, SHAP, white matter in HIV

## 1 | INTRODUCTION

Diffusion-weighted magnetic resonance imaging (MRI) techniques play a key role in assessing microstructural brain changes related to neurodegenerative diseases, characterizing neoplastic tissues and predicting and monitoring response to treatment (Assaf et al., 2019; Padhani et al., 2009).

While diffusion tensor imaging (DTI) is based on the assumption that the movement of water molecules within tissue is described by a Gaussian distribution (Novikov et al., 2019), biological matrices are dense with cellular and macromolecular structures, which effectively invalidates this assumption (Assaf & Pasternak, 2008). In this respect, a number of statistical models (e.g., the Diffusional Kurtosis model; Jensen et al., 2005) have been developed, which employ the higher cumulants of the diffusion probability density function to cater to non-Gaussian diffusion and/or non-monoexponential decay of the diffusion-weighted signal. While such models can provide high sensitivity, their specificity is often low owing to their purely statistical nature, and changes in the indices provided by such models can be explained by concomitant biological phenomena, rendering a biological interpretation of imaging findings arduous. An alternative approach to the interpretation of the diffusion-weighted signal is the use of biophysical models to obtain more specific biomarkers of tissue microstructure.

The Combined Hindered And Restricted Model of Diffusion (CHARMED) (Assaf & Basser, 2005) is a biophysical model that can be fitted using data compatible with clinically feasible scan times. CHARMED models the diffusion-weighted (DW) signal using two compartments (Assaf et al., 2004): an extra-axonal diffusion compartment, which models the DW signal originating from hindered diffusion, and an intra-axonal diffusion compartment, which represents the DW signal originating from restricted diffusion. A number of indices can be extracted from CHARMED, most notably the restricted fraction (FR), that is, the portion of the DW signal that the model explains through hindered diffusion. FR has been shown to be more sensitive to axonal integrity than DTI (Toschi et al., 2020) and can be very sensitive to various white matter (WM) pathologies involving myelin, axonal density or intra-axonal composition (de Santis, Bastiani, et al., 2019). CHARMED has been used to study various conditions, such as multiple sclerosis (de Santis, Granberg, et al., 2019; Toschi et al., 2019), WM microstructural changes in healthy aging (Toschi et al., 2020), putative axonal density changes in the human brain (de Santis et al., 2016), and microstructural assessment of plasticity dynamics (Tavor et al., 2013).

Several diffusion imaging techniques have been used to assess structural and ultrastructural changes in the central nervous system (CNS) of HIV-infected patients as well as to monitor the course of infection (Bell et al., 2018; Davies et al., 2019; Garaci et al., 2019; Li et al., 2018; O'Connor et al., 2017). Once HIV reaches the CNS, it causes inflammatory phenomena that involve brain networks in both white and gray matter, causing a plethora of neurological alterations

that also involve cognitive impairment (Behrman-Lay et al., 2016). Since it has been shown that these neurological abnormalities are associated with traditional DTI metrics (Correa et al., 2015; Heaps-Woodruff et al., 2016), we postulated that more advanced and specific models such as CHARMED may have greater utility in understanding the effects of HIV on tissue microstructure.

The aim of this study was to explore brain microstructural changes in HIV-infected patients using the CHARMED model to gain insight into compartment-specific changes in whole-brain white matter. We also explore whether statistical multishell models (and, in particular, DKI) are able to provide increased sensitivity and specificity to disease despite their lack of microstructural interpretability. Finally, we employed explainable machine learning methods based on gradient boosting to probe the predictive value of indices derived from CHARMED in discriminating subtle differences between HIV patients and healthy controls while providing insight into which brain regions contribute most to this prediction through explainability techniques.

## 2 | MATERIALS AND METHODS

The overall workflow of the study is shown in Figure 1.

### 2.1 | Study participants

Fifty-five participants were enrolled at the Department of Infectious Diseases of the University Hospital Rome "Tor Vergata." The study population included 35 HIV-positive patients without neurological impairment and 20 healthy controls. The present study was approved by the local ethics committee. Inclusion criteria were (a) previous HIV infection and (b) no clinical evidence of neurological disorders. Exclusion criteria: (a) history of head trauma, (b) stroke, (c) epilepsy, (d) CNS infections, (e) demyelinating disease, (f) tumors, (g) coinfections, (h) or any kind of contraindication to MRI examinations. The HIV-positive group comprised 27 men and eight women, with an average age of 41.3 years (range 24–65 years). Healthy controls were composed of 11 men and nine women, with an average age of 44.1 years (range 27–64 years). When comparing average age and sex between the HIV group and the healthy controls, we found no significant differences in age ( $p = 0.46$ , Mann-Whitney  $U$  test) or sex ( $p = 0.08$ , chi-square test).

### 2.2 | Magnetic resonance imaging protocol

MRI was performed with a 3 T system (Achieva 3 T Intera, Philips Healthcare, Best, The Netherlands) using an 8-channel phased array head coil. The gradient amplitude and rise time were 80 mT/m and 200 mT/m/ms, respectively. For all subjects, the MRI acquisition

protocol included an axial T2-weighted turbo spin echo sequence, axial T2-fluid attenuated inversion recovery, sagittal T1-weighted turbo spin echo sequence, and a T1-3D fast field echo sequence, which were used by expert neuroradiologists to exclude neuroradiological abnormalities. DWI was acquired using a spin-echo (SE) echo-planar (EPI) single-shot sequence with the following parameters: acquisition matrix,  $94 \times 94$ ; field of view,  $24 \times 24 \text{ cm}^2$ ; repetition time/echo time, 7774 ms/89 ms; slice thickness, 2.5 mm; slices, 60; and no gap; gradient duration  $\delta$  (ms) 35; diffusion time  $\Delta$  (ms) = 44. Three different  $b$  values (0, 1000, and 2500  $\text{s/mm}^2$ ) were used. Thirty-two noncoplanar and noncollinear directions were chosen for diffusion-weighted imaging ( $b = 1000, 2500 \text{ s/mm}^2$ ), and eight non-diffusion-weighted reference images ( $b = 0 \text{ s/mm}^2$ ) were also collected. The SENSE (SENSitivity Encoding) imaging option with a scan time reduction factor of 2 was used. The total scan time was 35 min.

### 2.3 | MRI data preprocessing and model fitting

DW were preprocessed using the eddy tool, part of FSL (FMRIB Software Library v.6.0.4, Oxford, UK; Jenkinson et al., 2012) to correct for subject motion and eddy currents. The Microstructure Diffusion Toolbox (MDT, <https://github.com/robbert-harms/MDT>) was used to fit both the DTI and CHARMED models through a Powell optimization procedure while using a cascade initialized optimization strategy (Harms et al., 2017; Harms & Roebroeck, 2018). Signal-to-noise ratio (SNR) calculations for each  $b$ -value were performed as described in (Veraart et al., 2016) in the mrtrix tool (<https://www.mrtrix.org/>) by averaging the estimated SNR voxelwise. Table S4 shows a decline in

SNR as a function of  $b$ -value, as expected. Reference images and images acquired with  $b = 1000 \text{ s/mm}^2$  were used to fit the DTI model and obtain fractional anisotropy (FA), mean diffusivity (MD) and radial diffusivity (RD). All  $b$ -values (0, 1000, and 2500  $\text{s/mm}^2$ ) were used to fit the CHARMED model using two possible fiber orientations per voxel (Harms et al., 2017; Harms & Roebroeck, 2018), after which the FR maps were calculated. In addition, another FR map was created by (1) fitting the charmed model with one, two or three possible fiber orientations and (2) selecting (for each subject) the FR value that corresponded to the lowest Akaike's information criterion (AIC) in each voxel. This led to a second version of the FR map ( $FR_{123}$ ), which employed the number of fibers (from one to three) that optimally fitted the diffusion-weighted signal in each voxel. Additionally, the diffusional kurtosis imaging (DKI) model was fitted using the same tools, from which mean kurtosis (MK) and radial kurtosis (RK) maps were extracted. Successively, regions of interest (ROIs) were defined using the ICBM-DTI-81 white matter labels Atlas (Mori et al., 2008; 48 ROIs across the whole brain), and mean values for all indices were calculated within each ROI.

### 2.4 | Statistical analysis

Tract-based spatial statistics (TBSS) (Smith et al., 2006) was used for voxelwise group comparison of all parameters to compare the HIV group to the control group. The TBSS analysis consists of the following steps: (a) nonlinear registration of all FA images with each other; (b) identification of the most representative FA image and use of this as the target image; (c) affine alignment of the target image in the

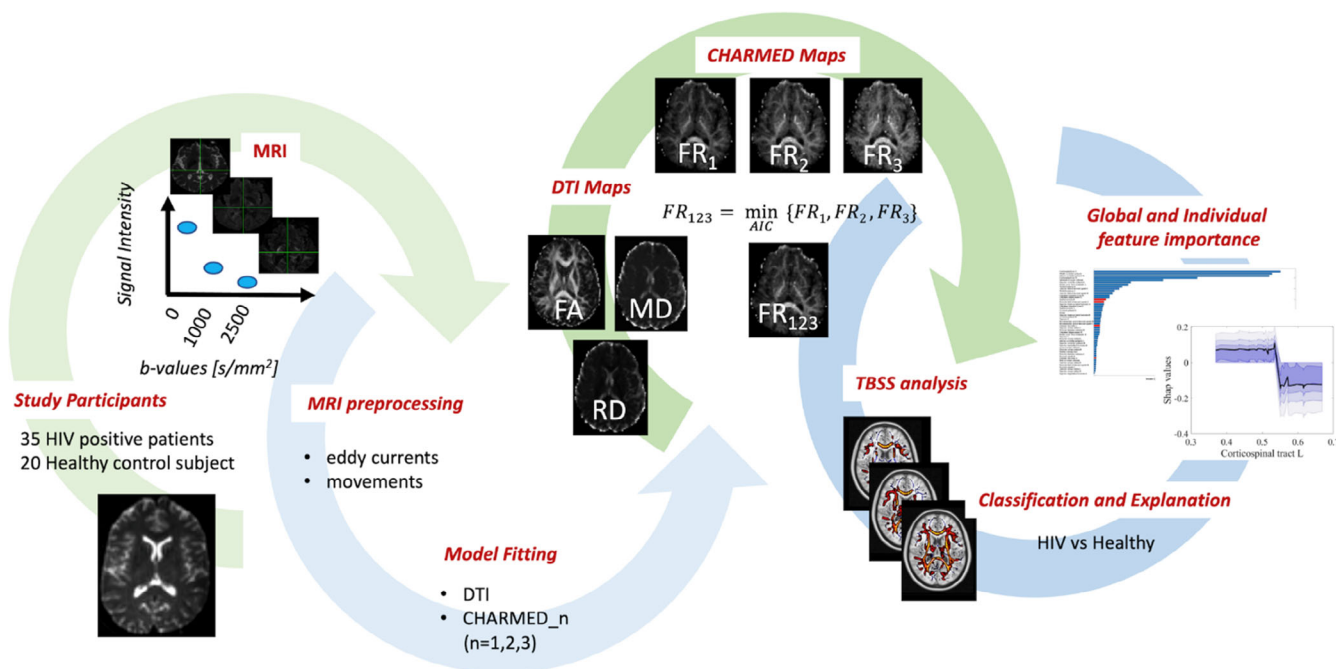


**FIGURE 1** Overall study workflow. DR, restricted fraction; DTI, diffusion tensor imaging; FA, fractional anisotropy;  $FR_{123}$ , Restricted fraction while choosing the number of fibers in each voxel between one and three according to Akaike's information criterion; MD, mean diffusivity; MRI, magnetic resonance imaging; RD, radial diffusivity; TBSS, tract-based spatial statistics. In addition to the indices depicted, mean kurtosis (MK) and radial kurtosis (RK) were also calculated.

Montreal Neurological Institute (MNI) 152 standard space; (d) transformation of each image into the MNI152  $1 \times 1 \times 1 \text{ mm}^3$  space by combining the nonlinear transformation of the target FA image with the affine transformation from that target to the MNI152 space; (e) creation of the mean of all FA images; (f) threshold at 0.2 and thinning to create an average FA skeleton; and (g) projection of each subject's aligned FA data onto this skeleton. Subsequently, all previously computed warps are applied to all maps (FA, RD, AD, FR, FR<sub>123</sub>), warping them into MNI space for subsequent skeletonization as described above. The skeletonization step improves robustness against between-subject registration errors. The resulting data were then fed into voxelwise intersubject, nonparametric statistics using the randomize tool, also part of FSL. For all diffusion-derived metrics (DTI, DKI, CHARMED), we tested the null hypothesis of no differences between the HIV-positive group and healthy control subjects using separate general linear models (GLMs), which included age and gender as nuisance covariates and correction for multiple comparisons over space using permutation-based nonparametric inference within the framework of the GLM (10,000 permutations) and using threshold-free cluster enhancement (TFCE) (Smith & Nichols, 2009), which eliminates the need for an arbitrary cluster threshold definition. A corrected  $p$  value  $<0.05$  was assumed to be statistically significant.

After TBSS, for each metric, we also calculated the percentage of voxels (out of the whole skeleton) in which a significant group effect was found. We also performed (a) ROI-wise statistical comparisons (Wilcoxon test) between groups (HIV patients vs. controls) of the median values of DWI-derived metrics and (b) classical AUC-ROC analysis calculated using multivariate logistic regression to provide direct comparison with the machine learning results (see below).

## 2.5 | Classification analysis and feature importance

Forty-eight ROIs across the whole brain for each metric (FA, MD, RD, RK, MK, FR, FR<sub>123</sub>) were used to train a nonlinear classifier in a machine learning (ML) framework using the extreme gradient boosting (XGBoost) algorithm (T. Chen & Guestrin, 2016) to discriminate HIV-positive-patients and healthy controls. XGBoost is a scalable end-to-end tree boosting algorithm that has shown state-of-the-art performance in a number of diverse machine learning applications (Olson et al., 2018). The complete dataset was split randomly into training (70%) and test (30%) sets. In the training set, hyperparameter values were optimized using a grid search in a 5-fold cross-validation scheme with the training set. After training, performance in the test set was assessed using an area under

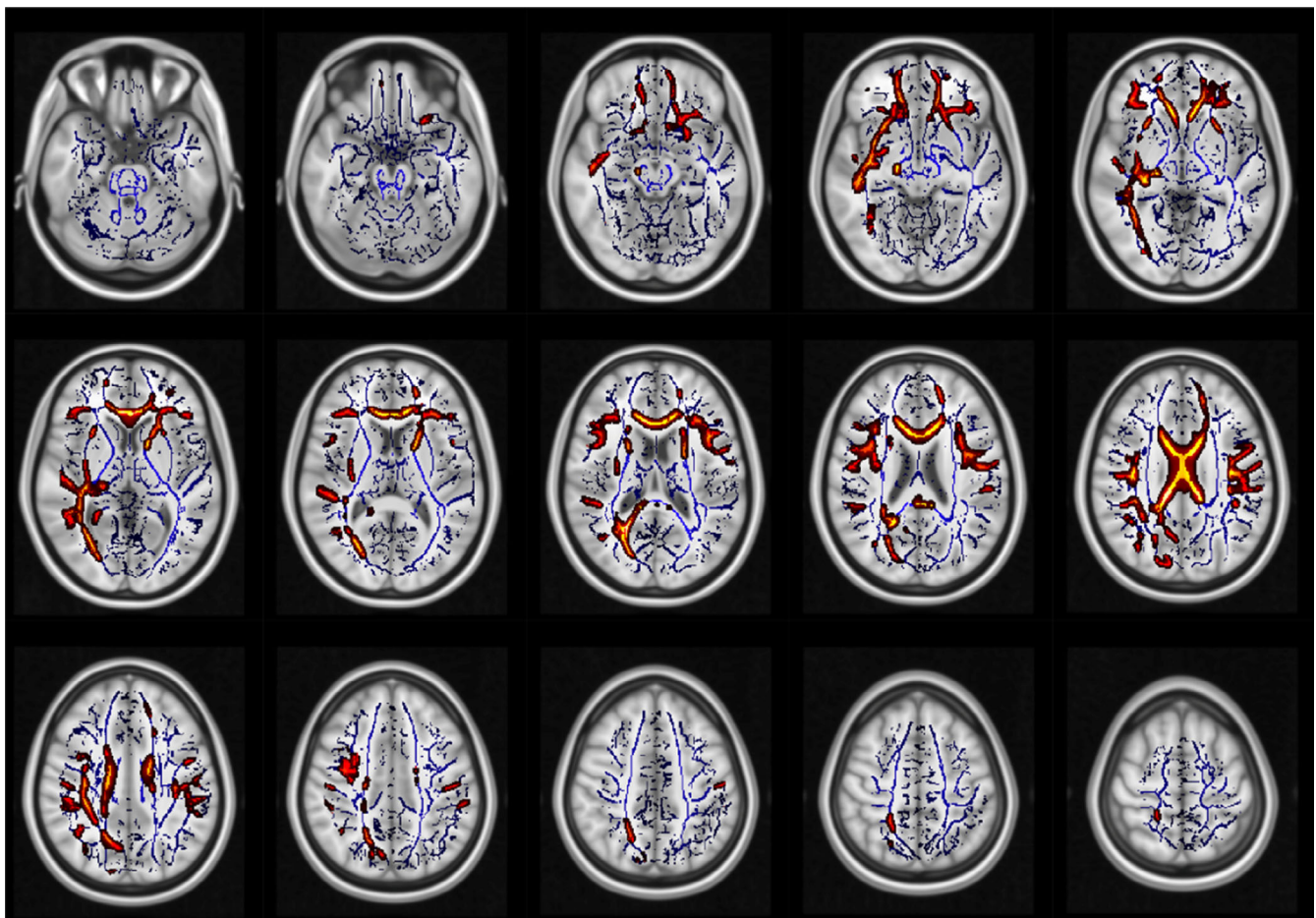


**FIGURE 2** White matter regions (red–yellow), which showed significantly lower FA in HIV patients than in controls. No significant results were found in the opposite contrast. Blue: white matter skeleton generated by the TBSS procedure.

the curve (AUC) metric assessed from the receiver operating characteristic (ROC) curve. Accuracy, sensitivity, specificity, F1-score and positive predictive value (PPV) were also computed. In addition, the contribution of each feature to the final prediction performance of the model was evaluated and ranked through Shapley Additive explanations (SHAP) values (Štrumbelj & Kononenko, 2013). SHAP values combine six existing methods for quantifying feature importance more consistently to human reasoning relative to previous machine learning explanatory approaches (Lundberg et al., 2020) and allow for quantification of both average and single-subject feature importance (i.e., unique contribution/importance of each feature in the final prediction). The splitting operation as well as all subsequent analyses were repeated 1000 times while changing the random seed to calculate the means and confidence intervals for all performance metrics. All participants provided written informed consent prior to the study.

### 3 | RESULTS

#### 3.1 | DTI analysis

The TBSS results showed significantly lower FA (Figure 2) values in HIV-positive patients than in healthy controls. In particular, we

observed lower FA values in HIV patients with moderate prevalence in the right brain hemisphere along the uncinate and superior longitudinal fasciculi, along the right inferior frontal-occipital bundle, left forceps minor and in the cingulate gyrus.

Additionally, MD (Figure S1) and RD (Figure S2) values were higher in HIV-positive patients than in healthy subjects. In the same comparison, MD and RD metrics showed higher values along the cingulate gyrus, right superior longitudinal fasciculus and along the U-fibers with slight right brain hemisphere prevalence; moreover, RD values were higher at the ganglionic level, and AD showed lower values in the right brain hemisphere along the inferior longitudinal fasciculus, the cortico-spinal tract, and the temporal part of the superior longitudinal and uncinate fasciculi. Finally, MK (Figure S3) and RK (Figure S4) were both lower in HIV-positive patients than in healthy subjects. These differences were widespread and involved the corpus callosum, cortico-spinal bundles, brainstem and middle cerebellar peduncle, cingulate gyrus and right superior longitudinal fasciculus.

#### 3.2 | CHARMED analysis

CHARMED analysis (Figures 3 and 4) revealed less focal and much more widespread involvement of brain tissue compared with DTI

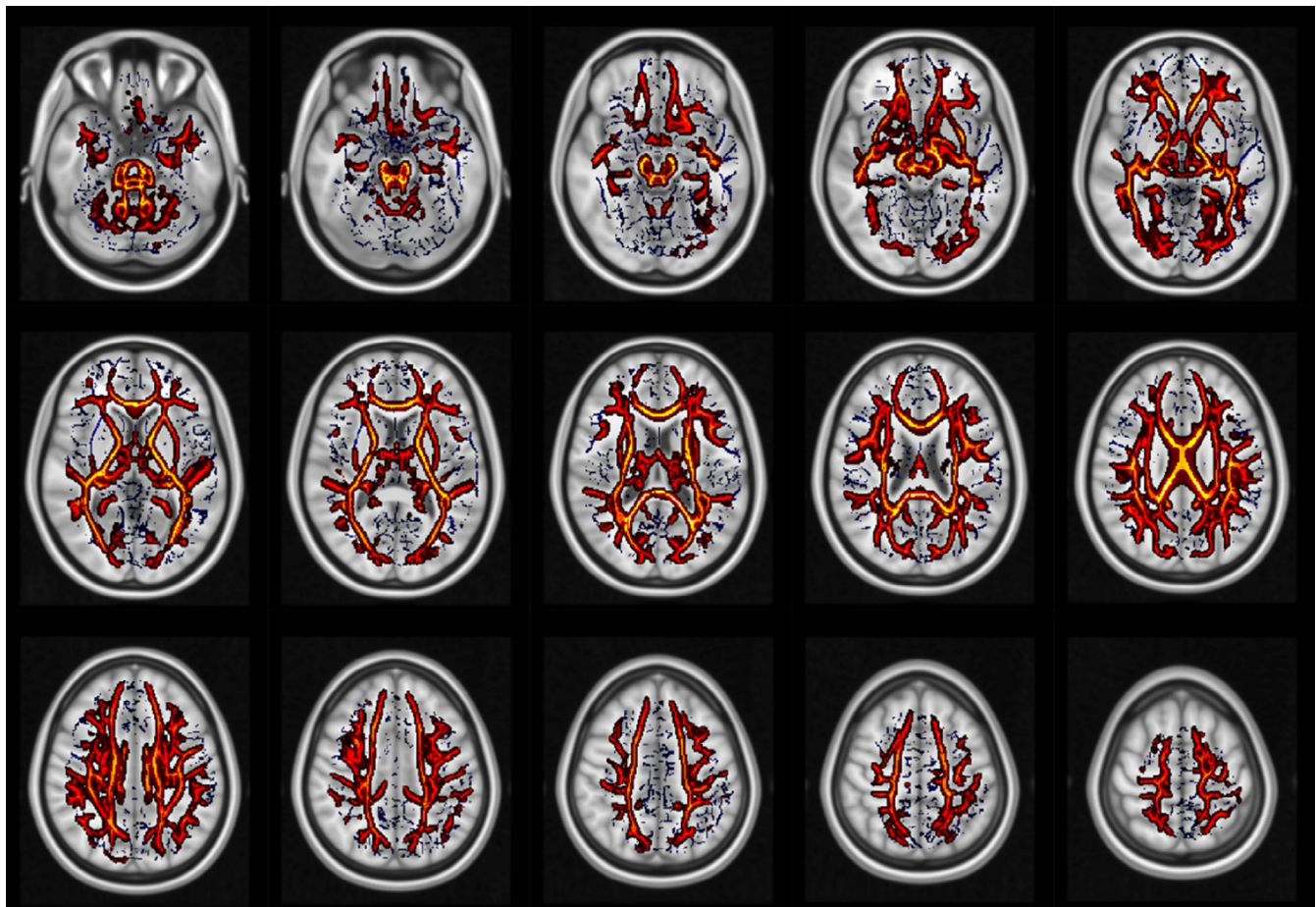


**FIGURE 3** White matter regions that showed significantly lower FR in HIV patients than in controls. No significant results were found in the opposite contrast. Blue: white matter skeleton generated by the TBSS procedure.

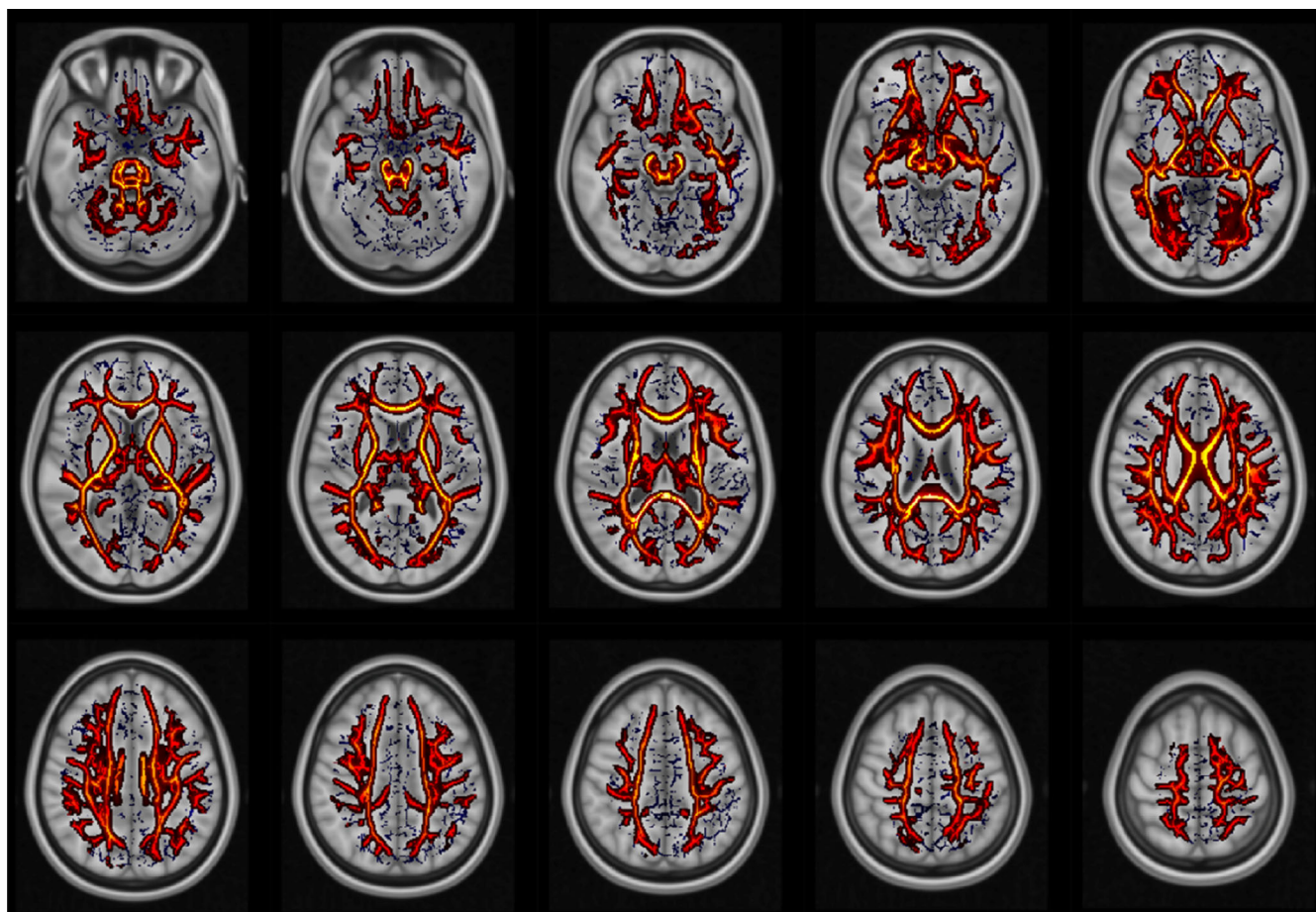


**FIGURE 4** White matter regions that showed significantly lower  $FR_{123}$  in HIV patients than in controls. No significant results were found in the opposite contrast. Blue: white matter skeleton generated by the TBSS procedure.

**TABLE 1** Spatial extent of statistically significant differences between HIV-positive patients and healthy controls. percentage of voxels (out of the whole skeleton) where we found significant group effects in TBSS analysis

Metric	%
FR	78.53
$FR_{123}$	85.94
FA	14.32
MD	24.97
RD	27.33
MK	88.42
RK	84.08

Abbreviations: FA, fractional anisotropy; FR, restricted signal fraction;  $FR_{123}$ , restricted signal fraction when selecting the optimal number of fibers through Akaike's information criterion in each voxel; MD, mean diffusivity; MK, mean kurtosis; RD, radial diffusivity; RK, radial kurtosis.

metrics, in a similar way to DKI metrics. In particular, lower FR values were found in HIV-infected patients (compared with controls) along the corpus callosum, cortico-spinal bundles, brainstem and middle cerebellar peduncle. In the  $FR_{123}$  map (Figure 4), additional regions with

significant differences were highlighted, such as the left superior cerebellar peduncle, the pontine crossing tract, the left posterior limb of the internal capsule, and the left and right medial lemniscus.

### 3.3 | Descriptive spatial statistics and machine learning

The overall percentage of volume (across the TBSS skeleton) in which we found statistically significant differences between HIV patients and healthy controls was greatest (by factor 3) in the FR and  $FR_{123}$  and maps compared with DTI estimates (see Table 1).

The results from our optimized machine learning model based on ROI-wise values are shown in Table 2. MK, RK,  $FR_{123}$ , and FR yielded superior discrimination performance (in all examined classifier performance indices) between HIV patients and controls (compared with DTI metrics), confirming the hypothesis of a superior discrimination performance of multishell techniques. These performances were further corroborated by the direct ROI-wise comparison in all DWI metrics (Table S1) and by the results of traditional AUC-ROC analysis (Table S2).

In sum, indices derived from multishell techniques showed the best discrimination performance. Given that indices derived from the

**TABLE 2** Mean and standard deviation (across 1000 repetitions of three classification procedures) of classifier performances when using features from restricted signal fraction (FR) and restricted signal fraction when selecting the number of fibers in the CHARMED model according to the AIC in each voxel (FR<sub>123</sub>) for fractional anisotropy (FA), mean diffusivity (MD), radial diffusivity (RD), mean kurtosis (MK), and radial kurtosis (RK).

	AUC	Accuracy	Sensitivity	Specificity	f1-score	PPV
FR	0.89 ± 0.07	0.90 ± 0.06	0.84 ± 0.13	0.94 ± 0.08	0.93 ± 0.05	0.92 ± 0.06
FR <sub>123</sub>	0.86 ± 0.07	0.88 ± 0.06	0.80 ± 0.15	0.93 ± 0.09	0.91 ± 0.05	0.90 ± 0.07
FA	0.68 ± 0.11	0.71 ± 0.10	0.60 ± 0.20	0.77 ± 0.13	0.77 ± 0.09	0.79 ± 0.09
MD	0.69 ± 0.10	0.72 ± 0.09	0.60 ± 0.19	0.78 ± 0.13	0.78 ± 0.08	0.79 ± 0.08
RD	0.70 ± 0.11	0.73 ± 0.10	0.60 ± 0.20	0.80 ± 0.13	0.79 ± 0.09	0.79 ± 0.09
MK	0.89 ± 0.08	0.90 ± 0.07	0.84 ± 0.15	0.93 ± 0.09	0.92 ± 0.06	0.92 ± 0.07
RK	0.87 ± 0.08	0.88 ± 0.06	0.83 ± 0.17	0.90 ± 0.08	0.90 ± 0.05	0.92 ± 0.08

CHARMED model are also able to aid in the interpretation of the underpinning microstructural changes, we chose these data as well as MK to calculate global and individual feature importance and interpretability. Figures 5 and 6 summarize feature importance rankings for the models using FR and MK, respectively, to discriminate HIV-positive patients from healthy control subjects, where larger values indicate a larger contribution to the prediction. The six most important ROIs in the FR and MK maps to discriminate HIV-positive patients from healthy control subjects were the left corticospinal tract, the middle cerebellar peduncle, the right inferior cerebellar peduncle, the right corticospinal tract, the splenium of corpus callosum and the left superior cerebellar peduncle (FR) and the right corticospinal tract, the middle cerebellar peduncle, the medial lemniscus, the pontine crossing tract, the left cerebral peduncle and the left corticospinal tract (for MK). Additionally, analyzing the individual importance of these “top six” regions revealed that prediction importance decreases with increasing FR value, with a qualitative threshold in importance at approximately FR = 0.5, and it also decreases with decreasing MK value, with a qualitative threshold around MK = 0.8.

## 4 | DISCUSSION

DWI techniques are useful for evaluating white matter abnormalities in a vast number of pathologies that involve the CNS. Our patient population comprised HIV-positive young adults (mean age: 41.3), hence minimizing confounding factors such as aging, neurological impairment or coinfection, and their characterization included radiological examination of infratentorial structures as well as brain stem. Overall, several previous studies based on classical DW imaging (i.e., the DTI model) found significant differences between HIV-positive patients and healthy control subjects in brain areas related to several cognitive domains, such as complex attention, memory, executive function, and perceptual motor function, and DKI parameters have been associated with blood biomarkers of disease severity in HIV (Garaci et al., 2019). In this study, HIV-positive patients appeared to have widespread WM changes that ranged up to approximately 80% of the total volume white matter tracts, and this result was only visible when using multishell imaging. The CHARMED model as well as the DKI model yielded superior classification ability when evaluating the performance of each metric in discriminating HIV patients

from controls. One of the advantages of CHARMED is the ability to provide information about multiple fiber orientations within the same voxel (Assaf et al., 2004), and FR measures may show increased sensitivity to WM changes due to biological processes regarding myelin, number of fibers or intraaxonal composition. On the other hand, the ability of the DKI model to lump the non-Gaussian part of the DW signal attenuation into scalar indices also provides high sensitivity, albeit without a clear relation to the microstructure. Given the heterogeneity of white matter tract orientations at the voxel scale, we repeated our main analyses while selecting the “optimal” (in a model fitting sense) number of fibers. Interestingly, the resulting FR<sub>123</sub> maps appeared to yield even greater voxelwise sensitivity (i.e., larger percentage of voxels with significant differences) than FR, although when reducing spatial resolution in ROI-wise aggregation and performing machine learning-based prediction, FR and FR<sub>123</sub> yielded similar performances. In the FR and MK maps, areas involved in HIV infections were found in the left corticospinal tract, middle cerebellar peduncle, right inferior cerebellar peduncle, right corticospinal tract, splenium of the corpus callosum and left superior cerebellar peduncle; in addition, in the FR<sub>123</sub> map, we found involvement of the left superior cerebellar peduncle, pontine crossing tract, left posterior limb of the internal capsule, and left and right medial lemniscus. These areas are involved in language, motor, equilibrium, behavior and proprioception, which support the integration of CNS multimodal areas that are frequently impaired in HIV-positive patients (Bell et al., 2018; Chanraud et al., 2010; Garaci et al., 2019; Gongvatana et al., 2009; McArthur et al., 2005). Importantly, most of these changes were not detected using conventional DTI metrics.

Our results also show an increased radial diffusivity in HIV patients compared with controls, which may be caused by an impairment of myelin sheaths. This is especially true in the anterior regions of the corpus callosum, mainly implied in the connection of the brain hemispheres and medial and lateral surface of the frontal lobes. Previous studies investigated changes induced by HIV in brain microstructure through standard DTI. Most of these studies have found a decrease in FA and an increase in MD/RD values in different regions (Chen et al., 2009; Leite et al., 2013; Pomara et al., 2001; Ragin et al., 2004; Stubbe-Drger et al., 2012). In particular, compared with controls, several papers have found (i) reduced FA values in the splenium (Filippi et al., 2001; Wu et al., 2006) and the genu of the corpus callosum (Filippi et al., 2001; Heaps-Woodruff et al., 2016; Thurnher

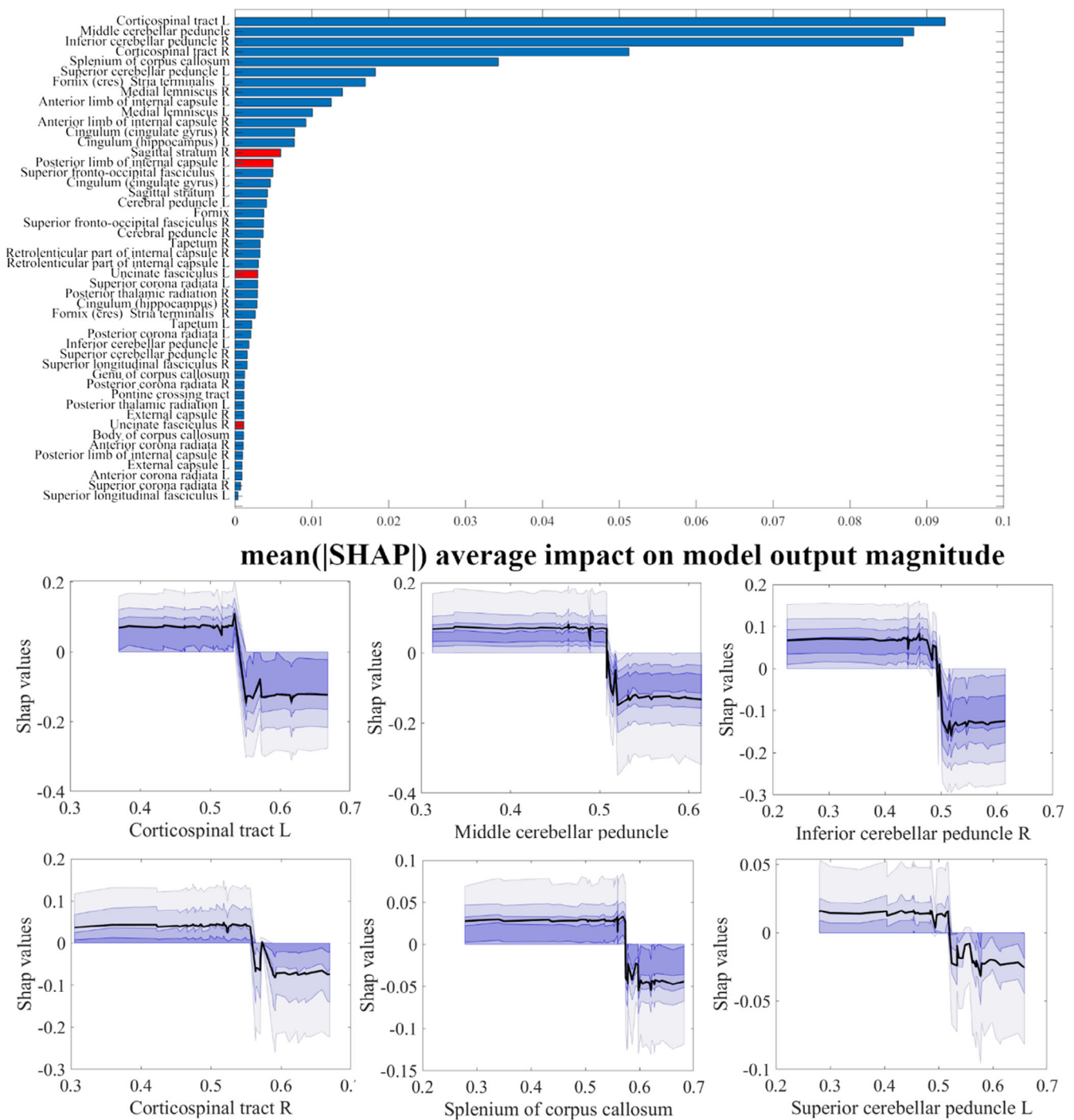


**FIGURE 5** Upper panel: ranking of ROI-wise FR values contributing to the discrimination of HIV-positive patients from healthy control subjects (SHAP values, averaged across the whole sample). Red bars represent ROIs with higher FR values in HIV patients, while blue bars represent the opposite. Lower panel: individual dependence of SHAP values (i.e., feature importance) on FR values in each of the top six ranking ROIs in the upper panel.

et al., 2005) and in frontal white matter (Pomara et al., 2001) and (ii) increased MD values in the genu (Thurnher et al., 2005) and splenium of the corpus callosum (Heaps-Woodruff et al., 2016; Wu et al., 2006). While our study confirms these trends in FA, MD and RD values, they appear to be localized in different areas of the brain, such as the corpus callosum, corticospinal tract, brainstem and

brachium pontis. Studywise differences could be due to a number of factors, such as differences in population size, treatment strategies (type, duration, efficacy, planning) as well as the MRI acquisition protocol and data analysis approach (O'Connor et al., 2017). For example, (Correa et al., 2015) reported no significant differences in the mean FA, MD, and RD values of WM bundles between controls and HIV-



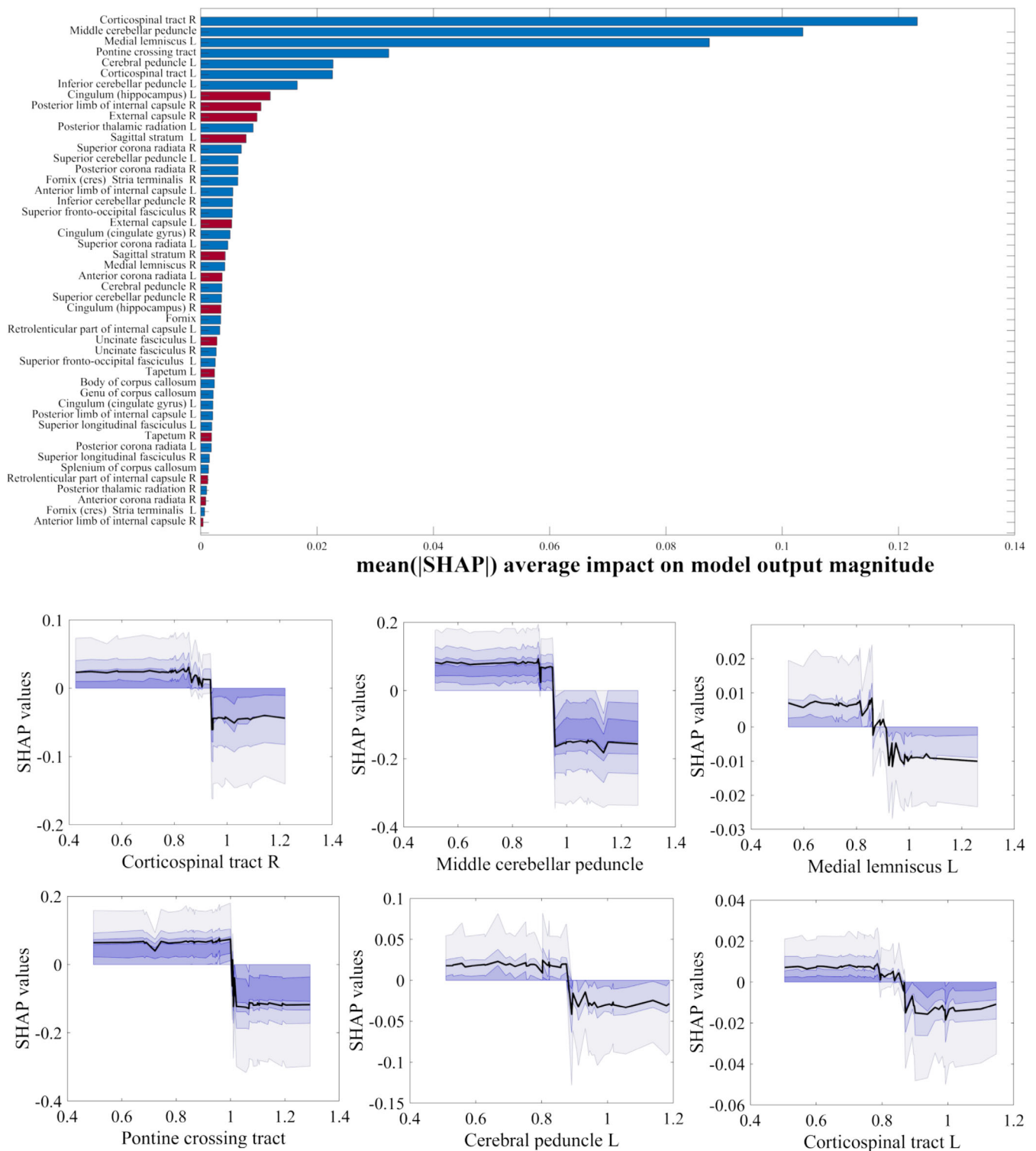


**FIGURE 6** Upper panel: ranking of ROI-wise MK values contributing to the discrimination of HIV-positive patients from healthy control subjects (SHAP values, averaged across the whole sample). Red bars represent ROIs with higher MK values in HIV patients, while blue bars represent the opposite. Lower panel: individual dependence of SHAP values (i.e., feature importance) on MK values in each of the top six ranking ROIs in the upper panel.

positive patients without planning deficits. That study used a relatively small patient population (13 patients without neurological impairment) and a lower field strength (1.5 T) compared with the

present study. In HIV-positive patients, most authors observed significant WM changes in frontal, temporal and occipital white matter, as well as associated white matter fiber tracts (Cilliers & Muller, 2021),

and recent studies have identified that the HIV group showed significantly higher MD and lower FA than the control group in the right corpus callosum, corona radiata, internal capsule, and posterior thalamic radiation; group differences in FA in these regions were also seen in the left hemisphere (Davies et al., 2019; Li et al., 2018). Additionally, previous studies explored the potential of DKI-derived metrics such as axonal water fraction and tortuosity in highlighting axonal damage in patients with HIV infection as well as multiple sclerosis (Buyukturkoglu et al., 2018) in the corpus callosum and anterior thalamic radiations, where these metrics were also associated with clinical test scores, pointing toward a clinical relevance of multishell DWI in HIV infection.

Additionally, in our machine learning analysis, the overall classification performance of  $FR_{123}$  was similar to that reached with FR as well as MK and RK. This implies that while voxelwise model selection may be useful in detecting slight differences, FR alone (in our case, derived from a two-fiber model) is a powerful discriminator of WM alterations, with higher performance than DTI metrics, even in a non-primarily neurological disease such as HIV infection. This conclusion is also supported by the use of modern explanation methods such as SHAP. When ranking brain regions according to importance in discriminating HIV patients from controls, the top six regions we found were the corticospinal tract (bilaterally), middle cerebral peduncle, inferior and superior cerebellar peduncles, and splenium of the corpus callosum, which showed high overlap with the top six regions contributing to the classification using DKI metrics. These regions are implicated in integrating proprioceptive sensory input with motor vestibular function, modulation of the contralateral homotopic and heterotopic areas of visual hierarchy and control of primary motor activity (Hall, 2012; Knyazeva, 2013).

Our study has some limitations. HIV-positive patients did not undergo neuropsychological testing, even though neurological symptoms were not detected. Additionally, the analyzed dataset is limited in size, although it compares favorably to previous DWI studies in HIV (Correa et al., 2015) (Heaps-Woodruff et al., 2016; Li et al., 2018). Consequently, our patients were not stratified further (e.g., our population was evaluated as a whole, independent of the Centers for Disease Control [CDC] classification of therapy status). Additionally, data about CNS penetration of antiretroviral drugs were not available. We were therefore not able to assess the correlation between CNS drug penetration and MRI parameters. Additionally, we chose not to apply heavy preprocessing, such as denoising or post hoc removal of Gibbs ringing, to balance the quality of preprocessing with the potential removal of information that it may lead to, also in view of the nonuniqueness of potential techniques to perform these steps. Nevertheless, all images were visually checked by experienced radiologists, and we could reasonably assume that acquisition artifacts would have, on average, affected both the HIV patients and the control group.

## 5 | CONCLUSIONS

When comparing HIV-infected patients to healthy controls, the CHARMED model showed markedly more widespread brain involvem

ent than the DTI model, also yielding a better overall discrimination performance. Similar results were attained by the DKI model, potentially validating the hypothesis that the main information carrier is the number of images and *b*-values used. The brain structures in which CHARMED- and DKI-related indices were significantly different in HIV patients compared with controls are related to multimodal associative brain areas whose functions (memory, attentive and emotional networks) are known to be often compromised in HIV-positive patients, hence offering a mechanistic explanation for these impairments. In addition, multishell imaging highlighted the involvement of the infratentorial structures, offering an additional explanation for motor impairments that might occur in HIV patients, and explainable AI methods allowed us to identify the dependence of the importance of CHARMED indices in the discrimination task on the value of the indices themselves.

The superior discrimination accuracy of indices derived from a multishell model within a clinically feasible scan time (approximately 18 min) allows us to envisage the use of neuroimaging-related biomarkers in HIV studies when monitoring brain involvement is needed; however, these results should be replicated in larger studies that also include the monitoring of cognitive functions.

## FUNDING INFORMATION

This work is supported by: #NEXTGENERATIONEU (NGEU) and funded by the Ministry of University and Research (MUR), National Recovery and Resilience Plan (NRRP), project MNESYS (PE0000006) (to NT)– A Multiscale integrated approach to the study of the nervous system in health and disease (DN. 1553 11.10.2022); by the MUR-PNRR M4C2I1.3 PE6 project PE00000019 Heal Italia (to NT); by the NATIONAL CENTRE FOR HPC, BIG DATA AND QUANTUM COMPUTING, within the spoke “Multiscale Modeling and Engineering Applications” (top NT); The European Innovation Council (Project CROSSBRAIN, Grant Agreement n. 101070908, Project BRAINSTORM, Grant Agreement 101099355); And by the Horizon 2020 research and innovation Programme (Project EXPERIENCE: Grant Agreement 101017727).

## CONFLICT OF INTEREST STATEMENT

All authors declare no conflict of interest.

## DATA AVAILABILITY STATEMENT

All data employed in this study are available upon reasonable request.

## ETHICS STATEMENT

The study was approved by the local ethics committee.

## ORCID

Nicola Toschi  <https://orcid.org/0000-0003-1929-5833>

## REFERENCES

- Assaf, Y., & Basser, P. J. (2005). Composite hindered and restricted model of diffusion (CHARMED) MR imaging of the human brain. *NeuroImage*, 27(1), 48–58. <https://doi.org/10.1016/j.neuroimage.2005.03.042>
- Assaf, Y., Freidlin, R. Z., Rohde, G. K., & Basser, P. J. (2004). New modeling and experimental framework to characterize hindered and restricted

- water diffusion in brain white matter. *Magnetic Resonance in Medicine*, 52(5), 965–978. <https://doi.org/10.1002/mrm.20274>
- Assaf, Y., Johansen-Berg, H., & Thiebaut de Schotten, M. (2019). The role of diffusion MRI in neuroscience. *NMR in Biomedicine*, 32(4), e3762. <https://doi.org/10.1002/nbm.3762>
- Assaf, Y., & Pasternak, O. (2008). Diffusion tensor imaging (DTI)-based white matter mapping in brain research: A review. *Journal of Molecular Neuroscience*, 34(1), 51–61. <https://doi.org/10.1007/s12031-007-0029-0>
- Behrman-Lay, A. M., Paul, R. H., Heaps-Woodruff, J., Baker, L. M., Usher, C., & Ances, B. M. (2016). Human immunodeficiency virus has similar effects on brain volumetrics and cognition in males and females. *Journal of Neurovirology*, 22(1), 93–103. <https://doi.org/10.1007/s13365-015-0373-8>
- Bell, R. P., Barnes, L. L., Towe, S. L., Chen, N. K., Song, A. W., & Meade, C. S. (2018). Structural connectome differences in HIV infection: Brain network segregation associated with nadir CD4 cell count. *Journal of Neurovirology*, 24(4), 454–463. <https://doi.org/10.1007/s13365-018-0634-4>
- Buyukturkdoglu, K., Fleyser, L., Byrd, D., Morgello, S., & Inglese, M. (2018). Diffusion kurtosis imaging shows similar cerebral axonal damage in patients with HIV infection and multiple sclerosis. *Journal of Neuroimaging*, 28(3), 320–327.
- Chanraud, S., Zahr, N., Sullivan, E. V., & Pfefferbaum, A. (2010). MR diffusion tensor imaging: A window into white matter integrity of the working brain. *Neuropsychology Review*, 20(2), 209–225. <https://doi.org/10.1007/s11065-010-9129-7>
- Chen, T., & Guestrin, C. (2016). XGBoost proceedings of the 22nd ACM SIGKDD international conference on knowledge discovery and data mining.
- Chen, Y., An, H., Zhu, H., Stone, T., Smith, J. K., Hall, C., Bullitt, E., Shen, D., & Lin, W. (2009). White matter abnormalities revealed by diffusion tensor imaging in non-demented and demented HIV+ patients. *NeuroImage*, 47(4), 1154–1162. <https://doi.org/10.1016/j.neuroimage.2009.04.030>
- Cilliers, K., & Muller, C. J. F. (2021). Effect of human immunodeficiency virus on the brain: A review. *Anatomical Record (Hoboken)*, 304(7), 1389–1399. <https://doi.org/10.1002/ar.24573>
- Correa, D. G., Zimmermann, N., Doring, T. M., Wilner, N. V., Leite, S. C., Cabral, R. F., Fonseca, R. P., Bahia, P. R., & Gasparetto, E. L. (2015). Diffusion tensor MR imaging of white matter integrity in HIV-positive patients with planning deficit. *Neuroradiology*, 57(5), 475–482. <https://doi.org/10.1007/s00234-015-1489-5>
- Davies, O., Haynes, B. I., Casey, S. J., Gerbase, S., Barker, G. J., Pitkanen, M., Kulasegaram, R., & Kopelman, M. D. (2019). Clinical and neuroimaging correlates of cognition in HIV. *Journal of Neurovirology*, 25(6), 754–764. <https://doi.org/10.1007/s13365-019-00763-w>
- de Santis, S., Bastiani, M., Droby, A., Kolber, P., Zipp, F., Pracht, E., Stoecker, T., Groppa, S., & Roebroeck, A. (2019). Characterizing microstructural tissue properties in multiple sclerosis with diffusion MRI at 7 T and 3 T: The impact of the experimental design. *Neuroscience*, 403, 17–26. <https://doi.org/10.1016/j.neuroscience.2018.03.048>
- de Santis, S., Granberg, T., Ouellette, R., Treaba, C. A., Herranz, E., Fan, Q., Mainero, C., & Toschi, N. (2019). Evidence of early microstructural white matter abnormalities in multiple sclerosis from multi-shell diffusion MRI. *NeuroImage: Clinical*, 22, 101699. <https://doi.org/10.1016/j.nicl.2019.101699>
- de Santis, S., Jones, D. K., & Roebroeck, A. (2016). Including diffusion time dependence in the extra-axonal space improves in vivo estimates of axonal diameter and density in human white matter. *NeuroImage*, 130, 91–103. <https://doi.org/10.1016/j.neuroimage.2016.01.047>
- Filippi, C. G., Ulug, A. M., Ryan, E., Ferrando, S. J., & van Gorp, W. (2001). Diffusion tensor imaging of patients with HIV and normal-appearing white matter on MR images of the brain. *AJNR. American Journal of Neuroradiology*, 22(2), 277–283.
- Garaci, F., Picchi, E., di Giuliano, F., Lanzafame, S., Minosse, S., Manenti, G., Pistolesse, C. A., Sarmati, L., Teti, E., Andreoni, M., Floris, R., & Toschi, N. (2019). Cerebral multishell diffusion imaging parameters are associated with blood biomarkers of disease severity in HIV infection. *Journal of Neuroimaging*, 29(6), 771–778. <https://doi.org/10.1111/jon.12655>
- Gongvatana, A., Schweinsburg, B. C., Taylor, M. J., Theilmann, R. J., Letendre, S. L., Alhassoon, O. M., Jacobus, J., Woods, S. P., Jernigan, T. L., Ellis, R. J., Frank, L. R., Grant, I., & Charter, G. (2009). White matter tract injury and cognitive impairment in human immunodeficiency virus-infected individuals. *Journal of Neurovirology*, 15(2), 187–195. <https://doi.org/10.1080/13550280902769756>
- Hall, J. E. (2012). Preface. In *Pocket companion to Guyton and Hall textbook of medical physiology* (pp. vii–viii). Elsevier.
- Harms, R. L., Fritz, F. J., Tobisch, A., Goebel, R., & Roebroeck, A. (2017). Robust and fast nonlinear optimization of diffusion MRI microstructure models. *NeuroImage*, 155, 82–96. <https://doi.org/10.1016/j.neuroimage.2017.04.064>
- Harms, R. L., & Roebroeck, A. (2018). Robust and fast Markov chain Monte Carlo sampling of diffusion MRI microstructure models. *Frontiers in Neuroinformatics*, 12, 97. <https://doi.org/10.3389/fninf.2018.00097>
- Heaps-Woodruff, J. M., Wright, P. W., Ances, B. M., Clifford, D., & Paul, R. H. (2016). The impact of human immune deficiency virus and hepatitis C coinfection on white matter microstructural integrity. *Journal of Neurovirology*, 22(3), 389–399. <https://doi.org/10.1007/s13365-015-0409-0>
- Jenkinson, M., Beckmann, C. F., Behrens, T. E., Woolrich, M. W., & Smith, S. M. (2012). Fsl. *NeuroImage*, 62(2), 782–790. <https://doi.org/10.1016/j.neuroimage.2011.09.015>
- Jensen, J. H., Helpert, J. A., Ramani, A., Lu, H., & Kaczynski, K. (2005). Diffusional kurtosis imaging: The quantification of non-gaussian water diffusion by means of magnetic resonance imaging. *Magnetic Resonance in Medicine*, 53(6), 1432–1440. <https://doi.org/10.1002/mrm.20508>
- Knyazeva, M. G. (2013). Splenium of corpus callosum: Patterns of interhemispheric interaction in children and adults. *Neural Plasticity*, 2013, 639430. <https://doi.org/10.1155/2013/639430>
- Leite, S. C., Correa, D. G., Doring, T. M., Kubo, T. T., Netto, T. M., Ferracini, R., Ventura, N., Bahia, P. R., & Gasparetto, E. L. (2013). Diffusion tensor MRI evaluation of the corona radiata, cingulate gyri, and corpus callosum in HIV patients. *Journal of Magnetic Resonance Imaging*, 38(6), 1488–1493. <https://doi.org/10.1002/jmri.24129>
- Li, R. L., Sun, J., Tang, Z. C., Zhang, J. J., & Li, H. J. (2018). Axonal chronic injury in treatment-naive HIV+ adults with asymptomatic neurocognitive impairment and its relationship with clinical variables and cognitive status. *BMC Neurology*, 18(1), 66. <https://doi.org/10.1186/s12883-018-1069-5>
- Lundberg, S. M., Erion, G., Chen, H., DeGrave, A., Prutkin, J. M., Nair, B., Katz, R., Himmelfarb, J., Bansal, N., & Lee, S. I. (2020). From local explanations to global understanding with explainable AI for trees. *Nature Machine Intelligence*, 2(1), 56–67. <https://doi.org/10.1038/s42256-019-0138-9>
- McArthur, J. C., Brew, B. J., & Nath, A. (2005). Neurological complications of HIV infection. *Lancet Neurology*, 4(9), 543–555. [https://doi.org/10.1016/S1474-4422\(05\)70165-4](https://doi.org/10.1016/S1474-4422(05)70165-4)
- Mori, S., Oishi, K., Jiang, H., Jiang, L., Li, X., Akhter, K., Hua, K., Faria, A. V., Mahmood, A., Woods, R., Toga, A. W., Pike, G. B., Neto, P. R., Evans, A., Zhang, J., Huang, H., Miller, M. I., van Zijl, P., & Mazziotta, J. (2008). Stereotaxic white matter atlas based on diffusion tensor imaging in an ICBM template. *NeuroImage*, 40(2), 570–582. <https://doi.org/10.1016/j.neuroimage.2007.12.035>
- Novikov, D. S., Fieremans, E., Jespersen, S. N., & Kiselev, V. G. (2019). Quantifying brain microstructure with diffusion MRI: Theory and parameter estimation. *NMR in Biomedicine*, 32(4), e3998. <https://doi.org/10.1002/nbm.3998>

- O'Connor, E. E., Jaillard, A., Renard, F., & Zeffiro, T. A. (2017). Reliability of white matter microstructural changes in HIV infection: Meta-analysis and confirmation. *AJNR. American Journal of Neuroradiology*, 38(8), 1510–1519. <https://doi.org/10.3174/ajnr.A5229>
- Olson, R. S., Cava, W. L., Mustahsan, Z., Varik, A., & Moore, J. H. (2018). Data-driven advice for applying machine learning to bioinformatics problems. *Biocomputing*, 2018, 192–203. [https://doi.org/10.1142/9789813235533\\_0018](https://doi.org/10.1142/9789813235533_0018)
- Padhani, A. R., Liu, G., Koh, D. M., Chenevert, T. L., Thoeny, H. C., Takahara, T., Dzik-Jurasz, A., Ross, B. D., van Cauteren, M., Collins, D., Hammoud, D. A., Rustin, G. J., Taouli, B., & Choyke, P. L. (2009). Diffusion-weighted magnetic resonance imaging as a cancer biomarker: Consensus and recommendations. *Neoplasia*, 11(2), 102–125. <https://doi.org/10.1593/neo.81328>
- Pomara, N., Crandall, D. T., Choi, S. J., Johnson, G., & Lim, K. O. (2001). White matter abnormalities in HIV-1 infection: A diffusion tensor imaging study. *Psychiatry Research*, 106(1), 15–24. [https://doi.org/10.1016/s0925-4927\(00\)00082-2](https://doi.org/10.1016/s0925-4927(00)00082-2)
- Ragin, A. B., Storey, P., Cohen, B. A., Edelman, R. R., & Epstein, L. G. (2004). Disease burden in HIV-associated cognitive impairment: A study of whole-brain imaging measures. *Neurology*, 63(12), 2293–2297. <https://doi.org/10.1212/01.wnl.0000147477.44791.bd>
- Smith, S. M., Jenkinson, M., Johansen-Berg, H., Rueckert, D., Nichols, T. E., Mackay, C. E., Watkins, K. E., Ciccarelli, O., Cader, M. Z., Matthews, P. M., & Behrens, T. E. (2006). Tract-based spatial statistics: Voxelwise analysis of multi-subject diffusion data. *NeuroImage*, 31(4), 1487–1505. <https://doi.org/10.1016/j.neuroimage.2006.02.024>
- Smith, S. M., & Nichols, T. E. (2009). Threshold-free cluster enhancement: Addressing problems of smoothing, threshold dependence and localisation in cluster inference. *NeuroImage*, 44(1), 83–98. <https://doi.org/10.1016/j.neuroimage.2008.03.061>
- Štrumbelj, E., & Kononenko, I. (2013). Explaining prediction models and individual predictions with feature contributions. *Knowledge and Information Systems*, 41(3), 647–665. <https://doi.org/10.1007/s10115-013-0679-x>
- Stubbe-Drger, B., Deppe, M., Mohammadi, S., Keller, S. S., Kugel, H., Gregor, N., Evers, S., Young, P., Ringelstein, E. B., Arendt, G., Knecht, S., Husstedt, I. W., & German Competence Network, H. A. (2012). Early microstructural white matter changes in patients with HIV: A diffusion tensor imaging study. *BMC Neurology*, 12(1), 23. <https://doi.org/10.1186/1471-2377-12-23>
- Tavor, I., Hofstetter, S., & Assaf, Y. (2013). Micro-structural assessment of short term plasticity dynamics. *NeuroImage*, 81, 1–7. <https://doi.org/10.1016/j.neuroimage.2013.05.050>
- Thurnher, M. M., Castillo, M., Stadler, A., Rieger, A., Schmid, B., & Sundgren, P. C. (2005). Diffusion-tensor MR imaging of the brain in human immunodeficiency virus-positive patients. *AJNR. American Journal of Neuroradiology*, 26(9), 2275–2281.
- Toschi, N., de Santis, S., Granberg, T., Ouellette, R., Treaba, C. A., Herranz, E., & Mainero, C. (2019). Evidence for progressive microstructural damage in early multiple sclerosis by multi-Shell diffusion magnetic resonance imaging. *Neuroscience*, 403, 27–34. <https://doi.org/10.1016/j.neuroscience.2019.01.022>
- Toschi, N., Gisbert, R. A., Passamonti, L., Canals, S., & de Santis, S. (2020). Multishell diffusion imaging reveals sex-specific trajectories of early white matter degeneration in normal aging. *Neurobiology of Aging*, 86, 191–200. <https://doi.org/10.1016/j.neurobiolaging.2019.11.014>
- Veraart, J., Novikov, D. S., Christiaens, D., Ades-Aron, B., Sijbers, J., & Fieremans, E. (2016). Denoising of diffusion MRI using random matrix theory. *NeuroImage*, 142, 394–406. <https://doi.org/10.1016/j.neuroimage.2016.08.016>
- Wu, Y., Storey, P., Cohen, B. A., Epstein, L. G., Edelman, R. R., & Ragin, A. B. (2006). Diffusion alterations in corpus callosum of patients with HIV. *AJNR. American Journal of Neuroradiology*, 27(3), 656–660.

#### SUPPORTING INFORMATION

Additional supporting information can be found online in the Supporting Information section at the end of this article.

**How to cite this article:** Minosse, S., Picchi, E., Conti, A., di Giuliano, F., di Cì, F., Sarmati, L., Teti, E., de Santis, S., Andreoni, M., Floris, R., Guerrisi, M., Garaci, F., & Toschi, N. (2023). Multishell diffusion MRI reveals whole-brain white matter changes in HIV. *Human Brain Mapping*, 44(15), 5113–5124. <https://doi.org/10.1002/hbm.26448>